SUPPLEMENTARY INFORMATION

Porous graphene-like carbon from fast catalytic decomposition of biomass for energy storage applications

Aurora Gomez-Martin[1,2,*], Julian Martinez-Fernandez[1,2], Mirco Ruttert[3], Martin Winter[3,4], Tobias Placke[3], Joaquin Ramirez-Rico[1,2,*]

[1] Dpto. Física de la Materia Condensada, Universidad de Sevilla, Avda. Reina Mercedes SN, 41012 Sevilla, Spain.

[2] Instituto de Ciencia de Materiales de Sevilla (CSIC-Univ. Sevilla), Avda. Américo Vespucio 49, 41092 Sevilla, Spain.

[3] University of Münster, MEET Battery Research Center, Institute of Physical Chemistry, Corrensstraße 46, 48149 Münster, Germany

[4] Helmholtz Institute Münster, IEK-12, Forschungszentrum Jülich GmbH, Corrensstraße 46, 48149 Münster, Germany

[*] Corresponding author. Email: agomez28@us.es, Tel: +34 9545 56423
[*] Corresponding author. Email: jrr@us.es, Tel: +34 9545 50963

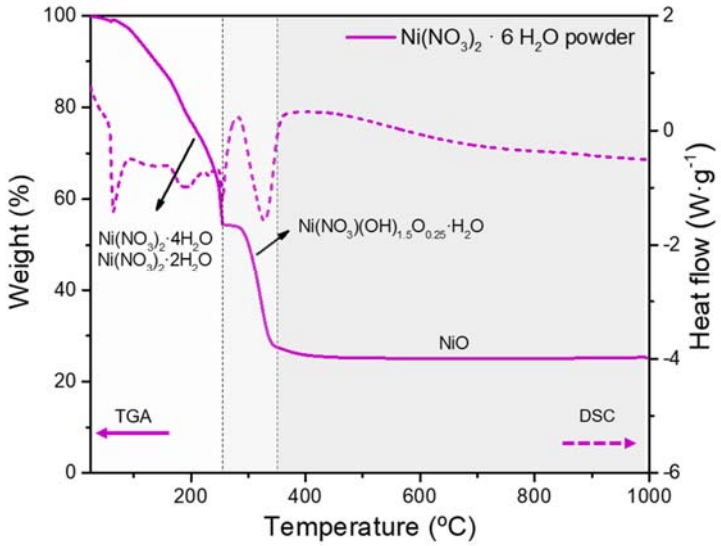

Figure S1. Representative TGA/DSC analysis of nickel nitrate hexahydrate powder. Weight change (left axis-solid line) and heat flow (right axis-dotted line) vs. temperature during heat treatment under a nitrogen flow rate of 100 ml·min^{-1} (heating rate of 10 ºC·min^{-1}). Different stages during thermal decomposition are highlighted by shaded grey areas. The thermal decomposition of nickel nitrate hexahydrate powder proceeds stepwise according to [1]: Water separation at 50 - 80 ºC [$Ni(NO_3)_2 \cdot 6H_2O = Ni(NO_3)_2 \cdot 4H_2O + 2H_2O$; $Ni(NO_3)_2 \cdot 4H_2O = Ni(NO_3)_2 \cdot 2H_2O + 2H_2O$]; partial decomposition steps at ≈ 150 - 250 ºC [oxidation and partial condensation; $Ni(NO_3)_2 \cdot 2H_2O = Ni(NO_3)(OH)_2 \cdot H_2O + NO_2$; $Ni(NO_3)(OH)_2 \cdot H_2O = Ni(NO_3)(OH)_{1.5}O_{0.25} \cdot H_2O + 0.25H_2O$]; and final oxide decomposition at ≈ 300 ºC [$Ni(NO_3)(OH)_{1.5}O_{0.25} \cdot H_2O = 0.5Ni_2O_3 + HNO_3 + 1.25H_2O$; $3Ni_2O_3 = 2Ni_3O_4 + 0.5O_2$; $Ni_3O_4 = 3NiO + 0.5O_2$].

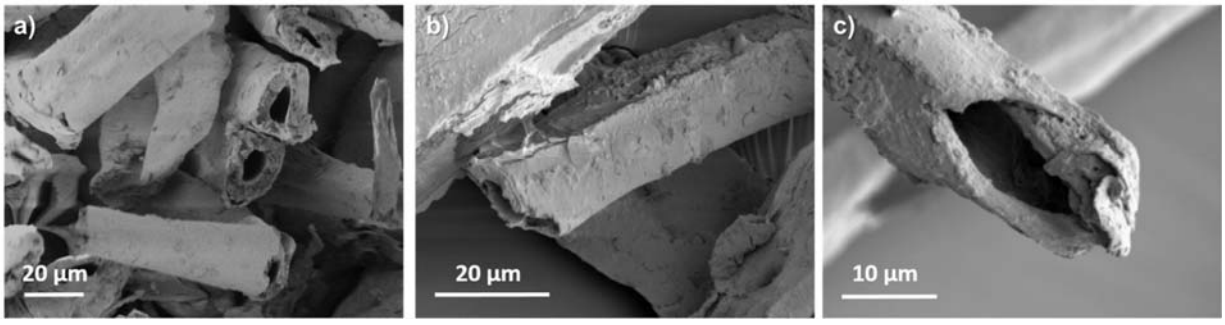

Figure S2. Representative SEM micrographs of: a) conventional non-treated MDF showing the compacted and pressed fibrous structure and b, c) MDF impregnated with an aqueous nickel nitrate solution before pyrolysis showing the debonding of cellulosic fibres but no change in fibre morphology.

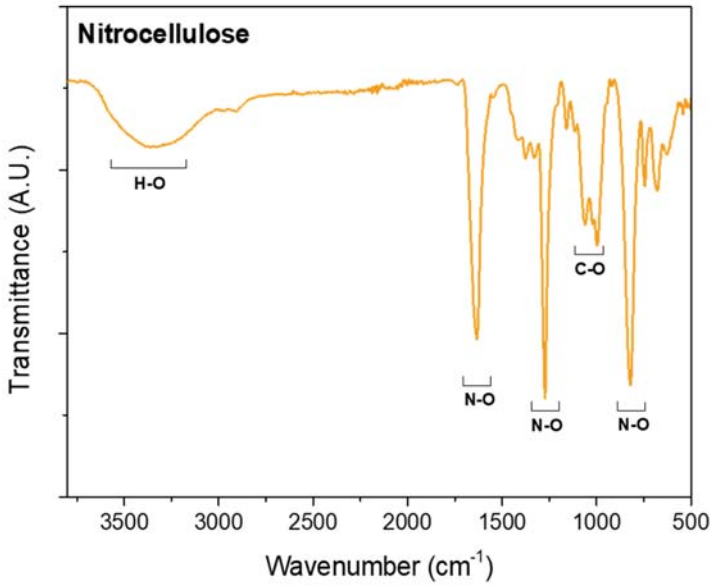

Figure S3. FTIR spectra of nitrocellulose synthetized by esterification of hydroxyl groups with nitric acid and sulphuric acid (weight ratio 1:3) of natural cotton.

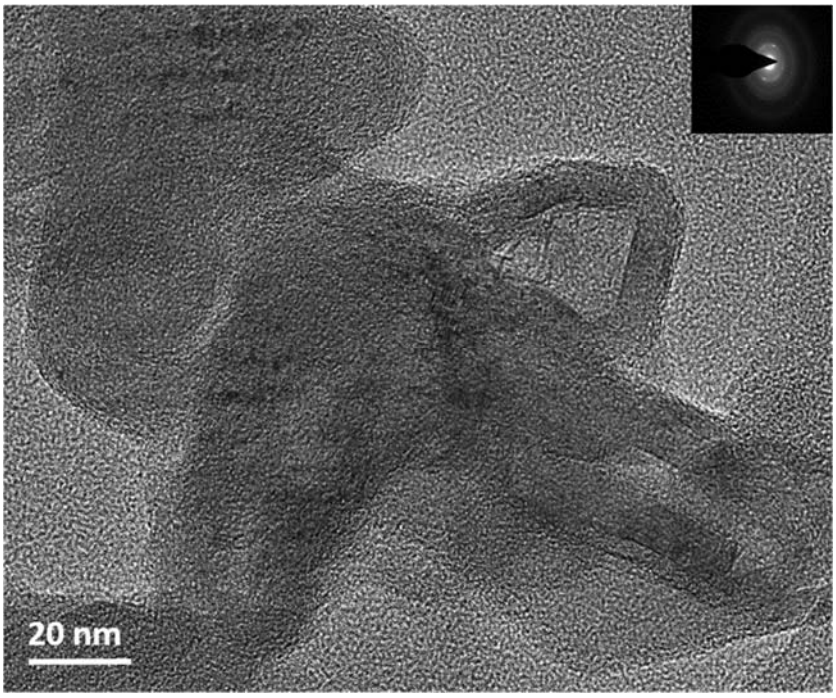

Figure S4. High-resolution TEM image and selected-area electron diffraction pattern (SAED) inset of a MDF sample impregnated with an aqueous nickel nitrate solution after pyrolysis up to 300 ºC.

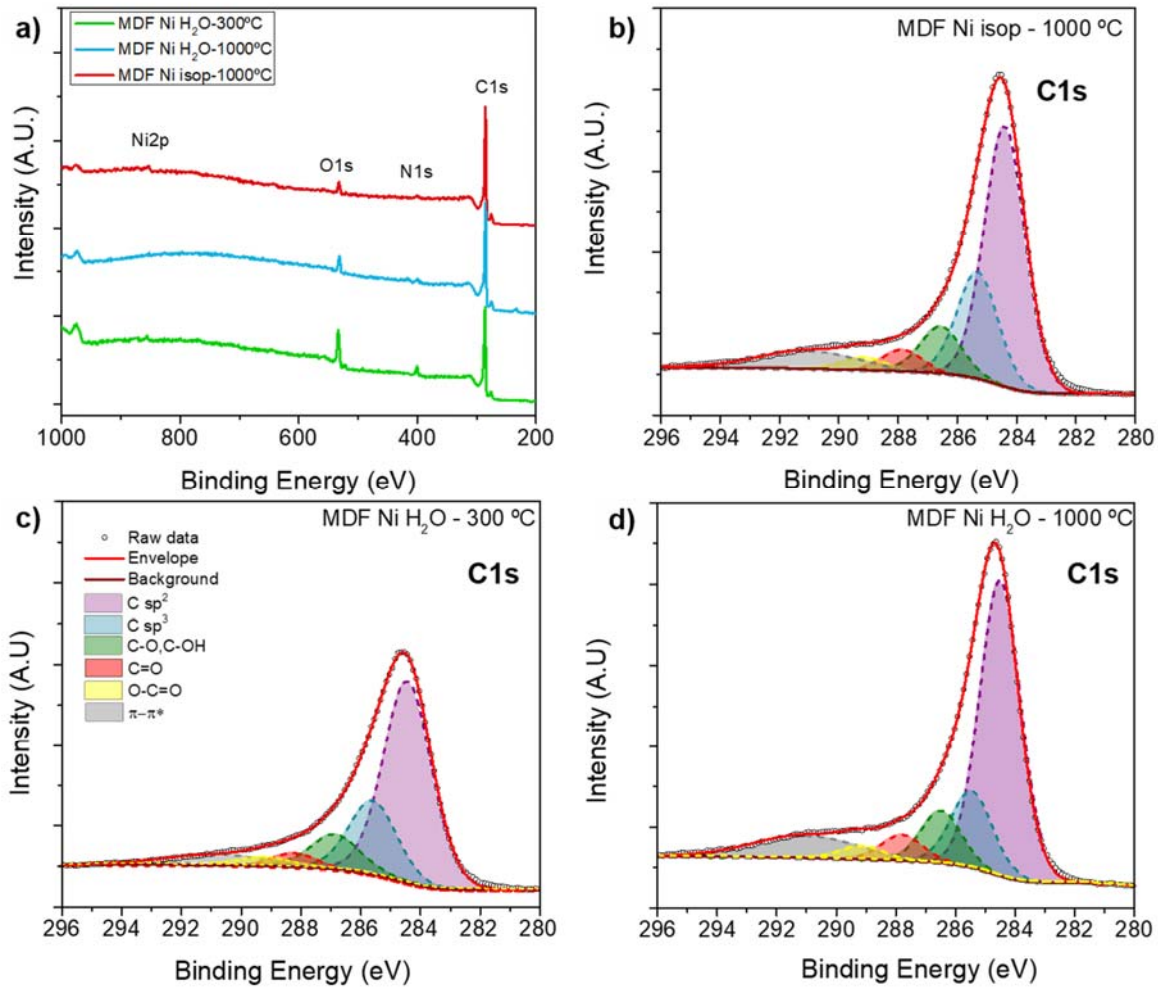

Figure S5. XPS spectra exhibiting characteristic peaks located at ≈285, 400, 533 and 855 eV, corresponding to C 1s, N 1s, O 1s and Ni 2p contributions, respectively. a) General XPS spectra and b, c, d) Results of C 1s spectra fitting of MDF Ni H_2O 300 and 1000 ºC compared to that of MDF Ni isop 1000 ºC.

Table S1. Comparison of specific capacitances of biomass-derived carbon materials as electrode for supercapacitor applications from this work and other previously reported carbon materials in aqueous electrolytes.

Biomass source	S_{BET} ($m^2 \cdot g^{-1}$)	Activation agent	Measurements conditions	Specific capacitance ($F \cdot g^{-1}$)	Rate capability, capacitance retention	Cycling stability, capacitance retention
Medium density fiberboard [This work]	333	$Ni(NO_3)_2$	Set-up: symmetric two-electrode Electrolyte: 6 M KOH Electrode mass: 5 mg Voltage range: 0 – 1 V	≈72 $F \cdot g^{-1}$ at 20 $mA \cdot g^{-1}$ (GCD experiment)	≈75 % at 100 $A \cdot g^{-1}$	≈96 % (10 000 cycles)
Coconut leaves [2]	493	CO_2	Set-up: symmetric two-electrode Electrolyte: 6 M KOH Electrode mass: --- Voltage range: 0 – 1 V	≈133 $F \cdot g^{-1}$ at 200 $mA \cdot g^{-1}$ (GCD experiment)	≈84 % at 5 $A \cdot g^{-1}$	≈74 % (10 000 cycles)
Chitin nanofibers [3]	256	HCl + freeze drying	Set-up: symmetric two-electrode Electrolyte: 6 M KOH Electrode mass: 0.61 mg Voltage range: 0 – 1 V	≈124 $F \cdot g^{-1}$ at 25 $mA \cdot g^{-1}$ (GCD experiment)	≈47 % at 50 $A \cdot g^{-1}$	----------
Cornstalks [4]	326	$K_4[Fe(CN)_6]$	Set-up: three-electrode Electrolyte: 6 M KOH Electrode mass: 5 mg Potential range: −1.1–0.1 V (vs. Hg/Hg_2Cl_2)	≈96 $F \cdot g^{-1}$ at 1 $A \cdot g^{-1}$ (GCD experiment)	≈70.5 % at 20 $A \cdot g^{-1}$	----------
Crab shells [5]	269	$FeCl_3$	Set-up: symmetric two-electrode Electrolyte: 6 M KOH Electrode mass: 2-3 mg Voltage range: 0 – 1 V	≈128.6 $F \cdot g^{-1}$ at 1 $A \cdot g^{-1}$ (GCD experiment)	≈70 % at 10 $A \cdot g^{-1}$	----------

Biomass source	S_{BET} ($m^2 \cdot g^{-1}$)	Activation agent	Measurements conditions	Specific capacitance ($F \cdot g^{-1}$)	Rate capability, capacitance retention	Cycling stability, capacitance retention
Glucose [6]	992	KOH + $Fe(NO_3)_3 \cdot 9H_2O$	Set-up: symmetric two-electrode Electrolyte: 6 M KOH Electrode mass: 1-2 mg Voltage range: 0 – 1 V	≈207 $F \cdot g^{-1}$ at 1 $A \cdot g^{-1}$ (GCD experiment)	≈78% at 50 $A \cdot g^{-1}$	≈83.7% (5000 cycles)
Rotten potatoes [7]	960	KOH	Set-up: symmetric two-electrode Electrolyte: 6 M KOH Electrode mass: 2 mg Voltage: 0 – 0.8 V	≈192 $F \cdot g^{-1}$ at 1 $A \cdot g^{-1}$ (GCD experiment)	≈53 % at 100 $A \cdot g^{-1}$	----------
Sheet cellulose [8]	539	Ball milling + KOH + freeze drying	Set-up: three-electrode Electrolyte: 6 M KOH Electrode mass: 2 mg Potential: -1.0 – 0 V (vs.Hg/HgO)	≈206 $F \cdot g^{-1}$ at 1 $A \cdot g^{-1}$ (GCD experiment)	≈39 % at 20 $A \cdot g^{-1}$	----------
Soybeans [9]	580	KOH	Set-up: symmetric two-electrode Electrolyte: 6 M KOH Electrode mass: 3 mg Voltage: 0 – 1 V	≈100 $F \cdot g^{-1}$ at 50 $mA \cdot g^{-1}$ (GCD experiment)	≈57 % at 20 $A \cdot g^{-1}$	----------
Sucrose [10]	691	Hydrothermal + $Ni(CH_3CO_2)_2 \cdot 4H_2O$	Set-up: symmetric two-electrode Electrolyte: 6 M KOH Electrode mass: --- Voltage: 0 – 1 V	≈248 $F \cdot g^{-1}$ at 50 $mA \cdot g^{-1}$ (GCD experiment)	≈85 % at 5 $A \cdot g^{-1}$	≈94 % (5000 cycles)
Sunflower seed shell [11]	619	KOH	Set-up: symmetric two-electrode Electrolyte: 30 wt. % KOH Electrode mass: 20 mg Voltage: 0 – 1 V	≈213 $F \cdot g^{-1}$ at 25 $mA \cdot g^{-1}$ (GCD experiment)	≈35 % at 10 $A \cdot g^{-1}$	------

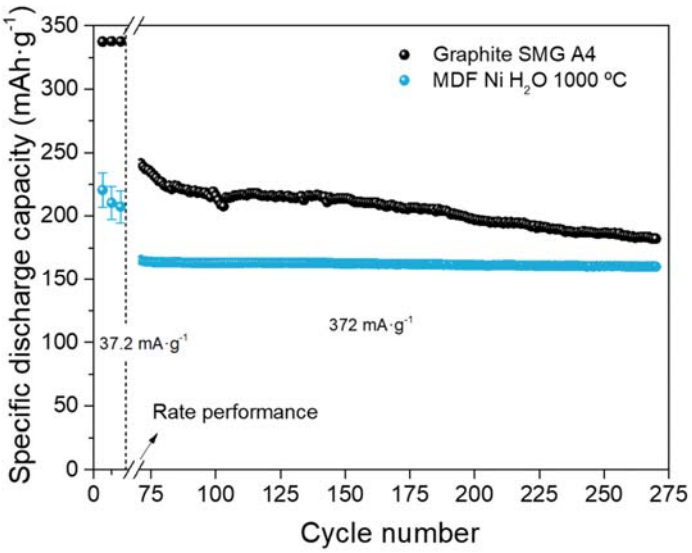

Figure S6. Cycling performance of a commercial SMG A4 graphite and MDF Ni H_2O 1000 ºC at specific current of 372 mA·g^{-1} for 200 cycles after the rate performance experiments.

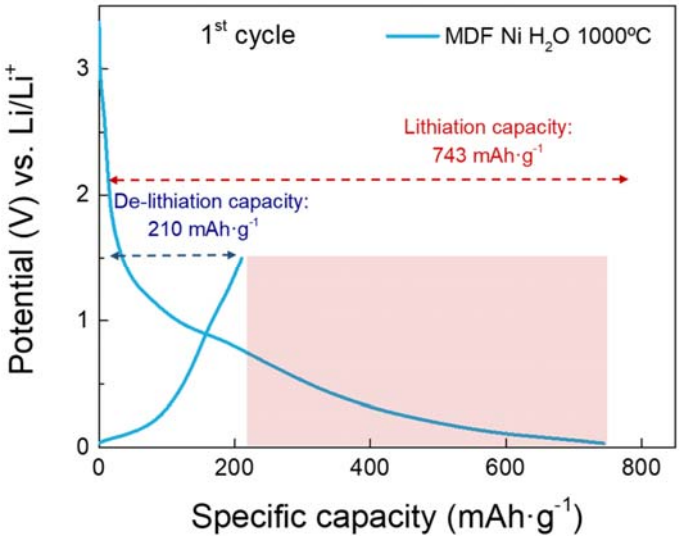

Figure S7. Representative constant-current potential profile (at a specific current of 37.2 mA·g^{-1}) for the 1st charge/discharge cycle. Red area shows the irreversible capacity between the first cycle charge/discharge capacities.

References:

1. Brockner, W.; Ehrhardt, C.; Gjikaj, M., Thermal decomposition of nickel nitrate hexahydrate, Ni(NO3)2·6H2O, in comparison to Co(NO3)2·6H2O and Ca(NO3)2·4H2O. *Thermochimica Acta* **2007,** *456* (1), 64-68.

2. Sulaiman, K. S.; Mat, A.; Arof, A. K., Activated carbon from coconut leaves for electrical double-layer capacitor. *Ionics* **2016,** *22* (6), 911-918.

3. Niu, Q.; Zhao, S.; Gao, K.; Wang, L., Natural nanofibers stacked porous nitrogen-doped carbon nanosheets with promising capacitive performance. *Cellulose* **2019,** *26* (9), 5395-5407.

4. Wang, L.; Mu, G.; Tian, C.; Sun, L.; Zhou, W.; Yu, P.; Yin, J.; Fu, H., Porous Graphitic Carbon Nanosheets Derived from Cornstalk Biomass for Advanced Supercapacitors. *ChemSusChem* **2013,** *6* (5), 880-889.

5. Shi, W.; Chang, B.; Yin, H.; Zhang, S.; Yang, B.; Dong, X., Crab shell-derived honeycomb-like graphitized hierarchically porous carbons for satisfactory rate performance of all-solid-state supercapacitors. *Sustainable Energy & Fuels* **2019,** *3* (5), 1201-1214.

6. Qin, J.; Zhu, S.; Feng, C.; Zhao, N.; Shi, C.; Liu, E.-Z.; He, F.; Ma, L.; Li, J.; He, C., In-situ space-confined catalysis for fabricating 3D mesoporous graphene and their capacitive properties. *Applied Surface Science* **2018,** *433*, 568-574.

7. Chen, X.; Wu, K.; Gao, B.; Xiao, Q.; Kong, J.; Xiong, Q.; Peng, X.; Zhang, X.; Fu, J., Three-Dimensional Activated Carbon Recycled from Rotten Potatoes for High-performance Supercapacitors. *Waste and Biomass Valorization* **2016,** *7* (3), 551-557.

8. Mo, R.-J.; Zhao, Y.; Zhao, M.-M.; Wu, M.; Wang, C.; Li, J.-P.; Kuga, S.; Huang, Y., Graphene-like porous carbon from sheet cellulose as electrodes for supercapacitors. *Chemical Engineering Journal* **2018,** *346*, 104-112.

9. Long, C.; Jiang, L.; Wu, X.; Jiang, Y.; Yang, D.; Wang, C.; Wei, T.; Fan, Z., Facile synthesis of functionalized porous carbon with three-dimensional interconnected pore structure for high volumetric performance supercapacitors. *Carbon* **2015,** *93*, 412-420.

10. Liu, T.; Liu, E.; Ding, R.; Luo, Z.; Hu, T.; Li, Z., Preparation and supercapacitive performance of clew-like porous nanocarbons derived from sucrose by catalytic graphitization. *Electrochimica Acta* **2015,** *173*, 50-58.

11. Li, X.; Xing, W.; Zhuo, S.; Zhou, J.; Li, F.; Qiao, S.-Z.; Lu, G.-Q., Preparation of capacitor's electrode from sunflower seed shell. *Bioresource Technology* **2011,** *102* (2), 1118-1123.